Optical Materials: X 25 (2025) 100400

Contents lists available at ScienceDirect

Optical Materials: X

journal homepage: www.journals.elsevier.com/optical-materials-x

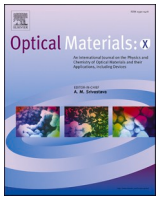

Charge trapping in SiO_2 substrate during electron beam deposition of CaF_2 thin films of different thicknesses

Marina Romanova [a,*], Sergii Chertopalov [b], Yuri Dekhtyar [a], Ladislav Fekete [b], Ján Lančok [b], Michal Novotný [b], Petr Pokorný [b], Anatoli I. Popov [c], Hermanis Sorokins [a], Aleksandr Vilken [a]

[a] Institute of Mechanical and Biomedical Engineering, Riga Technical University, Kipsalas Str. 6B, LV-1048, Riga, Latvia
[b] Institute of Physics, Czech Academy of Sciences, Na Slovance, 1999/2, Prague 8, 182 00, Czech Republic
[c] Institute of Solid State Physics, University of Latvia, 8 Kengaraga Str., LV-1063, Riga, Latvia

ARTICLE INFO

Keywords:
Calcium fluoride
Silicon dioxide
Electron beam deposition
Charge trapping
Electron irradiation
Photoelectron emission

ABSTRACT

The charge trapping phenomenon in the SiO_2 layer of Si/SiO_2 substrates during the electron beam deposition of CaF_2 thin films of varying thicknesses (50–277 nm) was studied. Photoelectron emission (PE) spectroscopy was employed to analyze electron trapping mechanisms induced by the deposition process. Distinct peaks corresponding to electron traps in the SiO_2 layer were identified in the PE spectra of CaF_2 films. The intensity of these peaks varied with the film thickness and the accumulated electron irradiation dose. The study also investigated the relaxation of the PE spectra in both vacuum and air environments. In a vacuum, the PE peaks and integrated PE intensity remained stable for at least 24 h for CaF_2 films of all thicknesses. When exposed to air, the PE peaks persisted for several days in films 125 nm thick or thinner but relaxed within several hours in 277 nm films. This rapid relaxation was attributed to a relatively high irradiation dose (about 2.5 mC) obtained during the fabrication of the 277 nm film, leading to an increased concentration of ionized F centers at the SiO_2–CaF_2 interface and the formation of (O^{2-}-V_A) centers upon air exposure. The relaxation of the PE spectrum intensity was attributed to electron transfer from SiO_2 traps to (O^{2-}-V_A) centers. Furthermore, the possibility of a 260 nm electron escape depth for CaF_2 material was confirmed.

1. Introduction

Calcium fluoride (CaF_2) is a wide-bandgap dielectric material that exhibits transparency across a broad range of wavelengths, from the infrared to the vacuum ultraviolet region [1–5]. This makes it an optimal material for optical components such as lenses and windows in the ultraviolet and infrared spectrum. The wide bandgap of CaF_2 provides resistance against photon-induced damage, making it a suitable material for use in harsh environments such as high-power lasers [6–8]. CaF_2 is also a key component in other applications, including radiation detectors, scintillators, solar cells, and microlithography processes for semiconductor manufacturing [9–16].

Defects in the crystal structure of CaF_2 can alter its optical properties [17–21]. Therefore, understanding the formation, diffusion, and charge state of these defects is crucial for predicting and mitigating changes in the optical behavior of CaF_2.

Silicon dioxide (SiO_2) is a substrate widely used for thin film deposition, including CaF_2 thin films [22,23]. Si/SiO_2 substrates, oxidized silicon wafers commonly used in microelectronics, can also be employed [24]. It has been demonstrated that the SiO_2 material becomes charged when exposed to accelerated electron irradiation, a phenomenon that has been modeled and experimentally confirmed in a number of studies [25–27]. This charging may also occur unintentionally during scientific manipulations, such as exposure to electron or ion beam irradiation in scanning electron microscopes (SEM) or focused ion beam (FIB) systems [28].

The phenomenon of charging is also observed during electron beam deposition of various thin films on SiO_2 substrates. In this process, electrons become trapped in the existing defect centers in the SiO_2 layer, affecting the properties of the deposited films. For example, the charge state of the substrate can affect the growth rate of the graphene-like films [29] and the characteristics of electronic devices fabricated on these substrates [30,31].

The present study employs the photoelectron emission (PE) technique to investigate electron trapping in the SiO_2 layer during electron beam deposition of CaF_2 thin films on Si/SiO_2 substrates. The charge

* Corresponding author.
E-mail address: marina.romanova@rtu.lv (M. Romanova).

https://doi.org/10.1016/j.omx.2025.100400
Received 20 November 2024; Received in revised form 26 December 2024; Accepted 6 January 2025
Available online 13 January 2025

transfer and trapping mechanisms are investigated, which are essential for designing devices using CaF_2 as a critical component. The results could provide insights into how deposition parameters and charge trapping in the substrate affect the optical performance of SiO_2/CaF_2 structures, with potential practical applications in photonics and optoelectronics.

2. Materials and methods

CaF_2 films with different thicknesses (50, 115, 125, and 277 nm) were deposited on oxidized silicon wafers (Si/SiO_2 substrates) using the electron beam evaporation technique. The substrates were prepared by growing a 1 μm thick SiO_2 layer on the (111) surface of a Si wafer at 1130 °C in an oxygen atmosphere. The substrate thickness was 0.35 mm. The substrates were then cut into squares with a side of approximately 8 mm and cleaned for 15 min using sonication, first in acetone and then in 2-propanol. Calcium fluoride powder (CaF_2, Aldrich 99.99 %, molar weight 78.07 g/mol) was used to prepare the pellets for deposition. The powder was placed into a 6 mm diameter vacuum pressing die, vacuumed for 10 min, and pressed at a pressure of 15 kN (1.5 tons) for 2 min under vacuum. The final step involved annealing the pellets at 800 °C in an argon gas flow furnace for 2 h, with a heating rate of 10 °C/min.

The prepared pellets were placed in a molybdenum (Mo) crucible of the electron beam evaporator (The e-flux Mini, Tectra GmbH) for deposition. The following deposition parameters were used: substrate temperature 235 °C, electron accelerating voltage 1 kV, filament current 7.6 A, electron beam current 23 mA, residual pressure in the chamber $5{\cdot}10^{-5}$ Pa, deposition pressure $2{\cdot}10^{-4}$ Pa. After deposition, the sample was allowed to cool to 55 °C in the deposition chamber. To ensure uniform film thickness, only one sample was deposited in the chamber at a time. The thickness and growth rate of the films were monitored using the IL150 Quartz Crystal Growth Rate Monitor (Intellemetrics Global Ltd.). After fabrication, the thickness of the films was confirmed using atomic force microscopy (Dimension Icon microscope, Bruker).

Fig. 1(a) shows the geometric arrangement of the crucible with a pellet, tungsten filament cathode, diaphragm, and substrate inside the deposition chamber. The dimensions of the deposition chamber components, the distances between them, and the applied electric potentials are shown in Fig. 1(b). These dimensions were used to analyze the electric fields generated in the deposition system during the deposition process.

The surface morphology of the deposited CaF_2 films was examined using atomic force microscopy (AFM). The measurements were performed with a Bruker Dimension Icon microscope equipped with Bruker ScanAsyst-Air probes that had a tip radius of 2 nm.

The phase composition of the CaF_2 films was characterized using an X-ray diffractometer (Empyrean, Malvern Panalytical) with Cu K<α> radiation (photon energy 8.04 keV, wavelength $\lambda = 1.54151$ Å, U = 45 kV, I = 30 mA). The measurements were carried out in a grazing incidence X-ray diffraction mode with an incidence angle of 0.85°, equivalent to an irradiation length of about 10 mm. Phase analyses were performed using HighScore Plus 4.6a software.

The elemental composition of the CaF_2 films was analyzed using X-ray photoelectron spectroscopy (XPS). Measurements were performed with an ESCALAB Xi + spectrometer (Thermo Scientific, Czech Republic) at a base pressure of less than 2×10^{-7} Pa in the analytical chamber. To eliminate potential contamination from air exposure, the top surface layer was removed by etching with monoatomic Ar^+ ions at an energy of 3000 eV for 10 s prior to analysis. Subsequent scans were performed, and the atomic percentage of detected elements was measured every 20 s of additional etching. The total etch time was 130 s, with an estimated etch rate of 0.86 nm/s (Ta_2O_5 equivalent).

The PE measurements of CaF_2 films and Si/SiO_2 substrates were conducted using a custom-built PE spectrometer in a vacuum of 10^{-3} Pa. The electron emission was excited by ultraviolet (UV) photons with energies ranging from 4.2 to 6.2 eV provided by a 30 W deuterium lamp (model L7296, Hamamatsu Photonics, Japan). A UV monochromator with automatic scanning (MDR-2, Russia) was used to select the wavelengths. Photoelectron emission current was detected using an SEM-6M secondary electron multiplier (VTC Baspik, Russia) connected to a Robotron 20046 radiometer (VEB Robotron-Meßelektronik, Germany) and an M8784 counting board (Hamamatsu Photonics, Japan). To determine the wavelength-dependent quantum yield of the UV source, an S1336-8BQ photodiode (Hamamatsu Photonics, Japan) was positioned at the sample location. The photocurrent at each wavelength was measured using a Keithley Model 6485 picoammeter. The spectral dependence of the number of quants per second of the UV source was determined using the known spectral response from the photodiode datasheet and the experimentally measured photocurrent dependence on the wavelength of light. The PE spectra were then corrected for this dependence.

This study involved two types of electron irradiation of $Si/SiO_2/CaF_2$

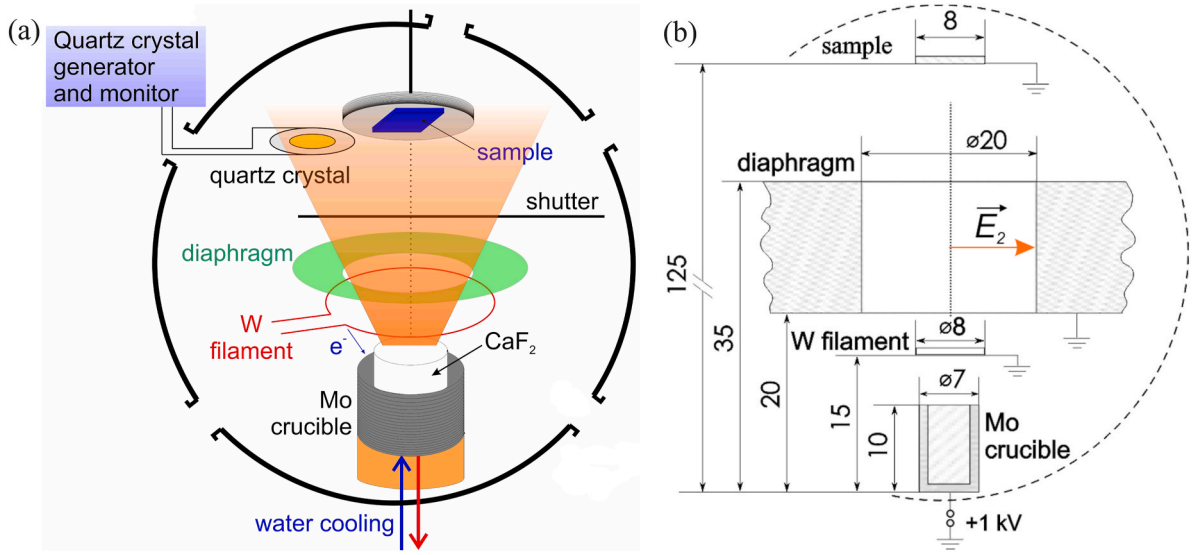

Fig. 1. Experimental setup for deposition: (a) schematic diagram of the deposition chamber; (b) dimensions and distances (in mm) between the crucible, tungsten filament, diaphragm, and deposited sample, as well as the applied electrical potentials. $\vec{E}_2$ is a radial electric field arising from the volume charge generated by electrons reflected from the crucible-pellet structure toward the substrate.

structures. The first type was electron irradiation that naturally accumulated during the electron beam deposition process of CaF_2 films. In this case, the electron dose was not independently controlled but was determined by the deposition time required to achieve the desired film thicknesses (50–277 nm). Consequently, thicker films corresponded to higher electron doses. The deposition time ranged from 104 to 803 s, corresponding to electron doses between 0.3 mC and 2.4 mC, based on the geometry of the deposition chamber.

The second type of irradiation involved additional electron exposure of the deposited CaF_2 films and bare Si/SiO_2 substrates in the vacuum chamber of the PE spectrometer. This controlled irradiation was performed to study the excitation and relaxation processes of the PE spectra. A custom-designed hot tungsten cathode source was used, with the sample positioned 4 cm from the cathode. The current density at the sample surface was approximately 0.3 μA/cm^2, with electron energies up to 1.5 keV. The irradiation time was varied to achieve different doses (up to 0.72 mC) in order to simulate additional charge trapping and explore the relaxation dynamics of the PE spectra in both vacuum and air environments.

3. Results and discussion

X-ray diffraction patterns (Fig. 2) demonstrate that the deposited CaF_2 films have a polycrystalline structure. The 50 nm thick film exhibits a face-centered cubic (FCC) structure (space group Fm-3m). Starting at a thickness of 115 nm, the CaO lime phase (chemical formula Ca_4O_4, reference code #96-100-0045) appears in the films. This phase also has an FCC structure (space group Fm-3m) [32]. The CaO phase content is less than 1 % for the 115 and 125 nm thick films. For the 277 nm thick film, 94 % of the CaF_2 phase and 6 % of the CaO phase are detected. No CaO lime phase is observed in the 50 nm thick film. The ratio of the intensities of the (111) and (022) reflections for the CaF_2 phase increases with film thickness, ranging from 0.83 for the 50 nm thick film to 2.12 for the 277 nm thick film. The 50 nm thick film is not textured. Texture growth along the <111> axis is observed for films starting at 115 nm thickness. The signal at 57.15° corresponds to the reflection from the Si(113) plane, and the halo peak at $2\theta = 21.05°$ corresponds to the amorphous SiO_2 phase of the substrate.

Fig. 3 shows the XPS survey spectrum of a 125 nm thick CaF_2 film as an example. The spectral features were identified using the internal element database of the data acquisition and processing software (Thermo Advantage v5.9931) and cross-referenced with the XPS database [34]. The spectrum reveals the presence of Ca, F, O, and Ar peaks. The atomic percentages of the detected elements were calculated from the survey spectra obtained during depth profiling using Ca2p, F1s, O1s, and Ar2p signals. The results showed that the element distribution remained uniform throughout the depth, with atomic percentages of 32.0 ± 0.3 at.% for Ca, 62.1 ± 0.3 at.% for F, 3.9 ± 0.3 at.% for O, and 1.9 ± 0.2 at.% for Ar. The ± values represent one standard deviation from the mean of measurements taken during depth profiling process. The presence of Ar contamination is attributed to the use of the Ar + gun for surface etching during XPS analysis.

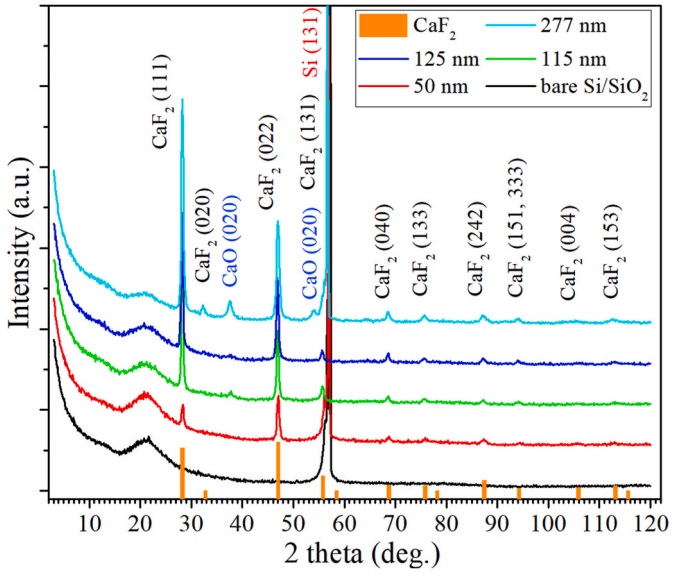

Fig. 2. XRD patterns of CaF_2 films and Si/SiO_2 substrate obtained in the grazing incidence mode, with reflexes for the CaF_2 powder from literature (X-ray database [33] (Reference code #00-035-0816)) shown for comparison. Thicknesses of CaF_2 films are given.

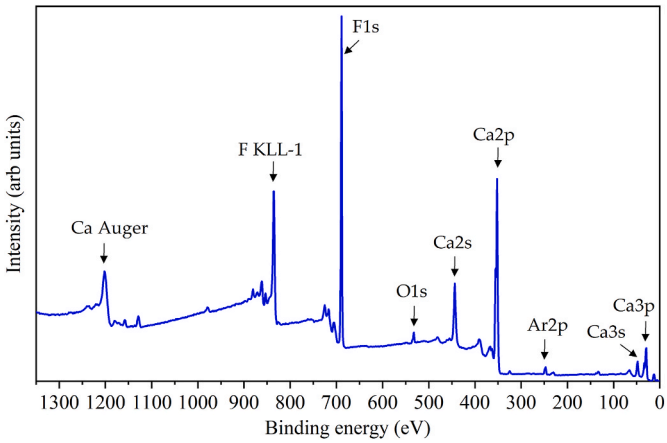

Fig. 3. XPS survey spectrum of a 125 nm thick CaF_2 film deposited on a Si/SiO_2 substrate, with individual core-level signals of the detected elements labeled.

Fig. 4 shows the AFM image of the surface of the CaF_2 film on the Si/SiO_2 substrate and its diagonal cross-section. The root mean square (RMS) roughness of the deposited films was calculated from the AFM images of 1 × 1 μm size and was found to be 2.8 ± 0.9 nm.

Fig. 5 shows the PE spectra of CaF_2 films of different thicknesses and the spectrum of a bare Si/SiO_2 substrate for comparison. The spectra of 50–125 nm thick CaF_2 films exhibit sharp PE peaks. These peaks are weakly pronounced in the spectrum of the thickest film (277 nm). The PE peaks are absent in the spectrum of the bare Si/SiO_2 substrate.

The peaks observed in Fig. 5 may initially suggest that they are characteristic of CaF_2 films. However, our previous research [35] demonstrated that the same PE peaks were observed in the spectra of bare Si/SiO_2 substrates after electron irradiation. This indicates that the Si/SiO_2 substrates may have been exposed to electrons during the deposition of the CaF_2 films using an electron beam. Consequently, the observed PE peaks in Fig. 5 could be attributed to photoemission from the Si/SiO_2 substrate through the CaF_2 film.

To test this hypothesis, bare Si/SiO_2 substrates were irradiated with 1.5 keV electrons in the vacuum chamber of the PE spectrometer. The spectra of the substrates before and after electron irradiation in Fig. 6 show PE peaks similar to those in Fig. 5, with the amplitudes of the peaks increasing with longer irradiation times. The irradiation time of 60 min corresponds to the dose of $q = 1.08$ mC. The photon energies of the peaks in Figs. 5 and 6 align within the measurement error, indicating that the $Si/SiO_2/CaF_2$ structure was subjected to electron irradiation during the deposition of CaF_2 films, and the PE spectra recorded from CaF_2 films are primarily determined by the photoemission of electrons trapped inside the SiO_2 layer of the $Si/SiO_2/CaF_2$ structure during the deposition process.

In the work [35] mentioned above, the appearance of PE peaks in the spectra of the irradiated Si/SiO_2 substrates is explained by the emission of electrons captured in pre-existing electron traps within the SiO_2 layer during electron irradiation. The electrons are emitted due to the Auger

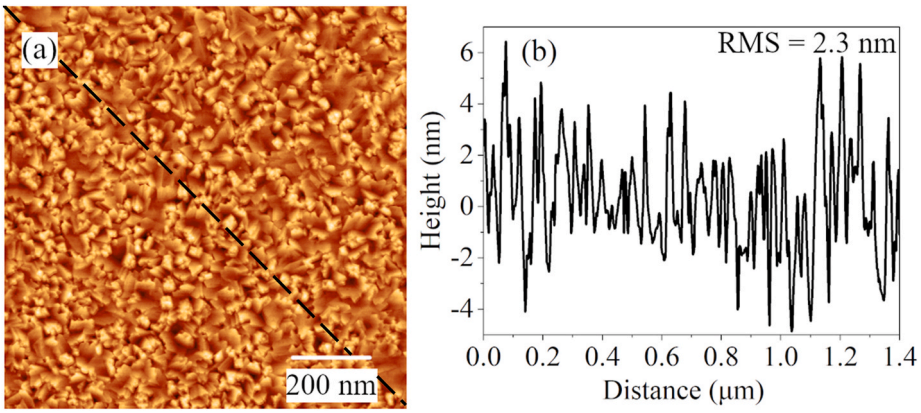

Fig. 4. AFM characterization of CaF_2 film on Si/SiO_2 substrate: (a) surface image of the film and (b) its diagonal cross-section profile along the dashed line in (a). The 115 nm thick film is shown as an example and its RMS roughness is also indicated in (b).

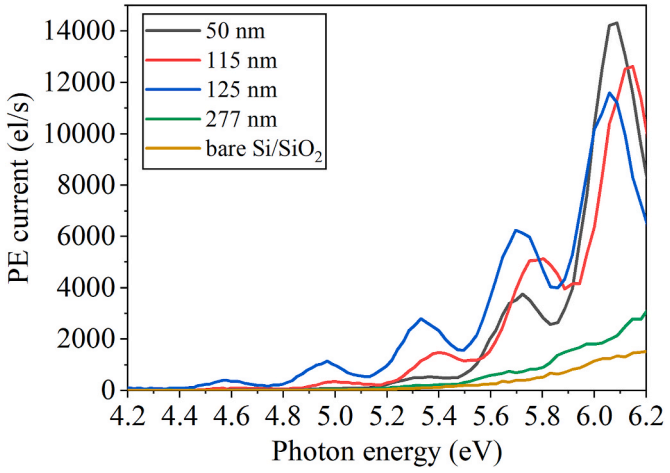

Fig. 5. PE spectra of CaF_2 films with various thicknesses and a bare Si/SiO_2 substrate.

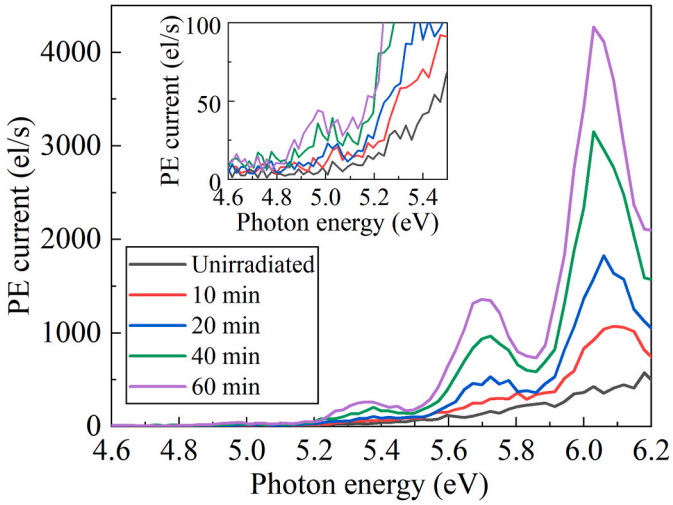

Fig. 6. PE spectra of the bare Si/SiO_2 substrate before and after irradiation with 1.5 keV electrons.

effect. First, an electron is excited by light from the ground state of a point defect in the SiO_2 layer at a wavelength characteristic of this type of defect. The energy of the excited electron is then transferred non-radiatively to other trapped electrons. If the transferred energy exceeds the ionization energy of the trapped electron, it is emitted into the vacuum. Since the excitation of a defect involves the absorption of a quantum of light through a resonant process, peaks are observed in the PE spectra.

To consider the possibility of irradiating $Si/SiO_2/CaF_2$ structures with electrons during the deposition of CaF_2 films, the electric fields generated in the deposition system during the deposition process are examined. The deposition system exhibits cylindrical symmetry, with a vertical axis passing through the centers of the annular cathode, crucible, and diaphragm (Fig. 1(a) and (b)). The metal crucible is at a potential of +1000 V relative to the cathode, which causes electrons to move from the cathode to the crucible along an imaginary cylindrical surface. These moving electrons can generate a direct current (DC) electric field oriented towards the center of the imaginary cylinder (the field of the imaginary cylindrical surface). This field can be described by calculations in an electrostatic field. While the nature of the DC electric field and the electrostatic field differs, both are potential fields characterized by a vector of intensity $\vec{E}$. In the case of a DC electric field, the charge distribution remains constant over time. However, if the charge distribution remains constant, the electric field generated by this charge is identical to the electrostatic field of the corresponding stationary charge distribution. Consequently, the results of calculations in the electrostatic field can be used to describe the field of the imaginary cylindrical surface.

During the deposition of CaF_2 films, a flux of high-energy electrons emitted from the cathode strikes the surface of the crucible and pellet, heating them to the vaporization temperature of CaF_2. However, some of these electrons are reflected from the crucible-pellet structure toward the substrate, generating a volume charge in the region between the pellet and the cathode.

The total electric field strength in the region between the pellet and the cathode is the sum of two electric field strengths: $\vec{E}_1$ and $\vec{E}_2$. The field strength $\vec{E}_1$ results from the flow of electrons along the imaginary cylindrical surface and is zero due to the cylindrical symmetry. The field strength $\vec{E}_2$ results from the volume charge of the reflected electrons (Fig. 1(b)) and can be calculated using equation (1) [36]:

$$\vec{E}_2 = \rho(v)\vec{r} \Big/ 2\varepsilon_0, \tag{1}$$

where ρ is the volume charge density, v is the electron velocity, $\vec{r}$ is the coordinate vector directed along the cylinder radius, and ε_0 is the electric constant.

Equation (2) gives the density (j) of the current that generates the volume charge in the cylinder [36]:

$$j = \rho(\upsilon) \cdot \upsilon \quad (2)$$

Some of the secondary electrons reflected from the crucible-pellet structure will enter the region bounded by the imaginary cylindrical surface. These electrons will be affected by the $\vec{E}_2$ field directed along the radius of this surface. The above equations indicate that slow electrons will have a higher volume charge density ρ, and the field strength at the edges of the cylinder will have a greater absolute value. Estimates from equations (1) and (2) show that electrons with an energy of 3 eV near the cylinder surface experience a field strength $\vec{E}_2$ of about 200 V/cm, while for electrons with an energy of 900–1000 eV, $\vec{E}_2$ is about 2 V/cm. Due to the linear relationship between the field strength $\vec{E}_2$ and the cylinder radius r and the stronger influence of the field on the slow part of the electron energy distribution, a small fraction of the secondary electrons will leave the cylinder region. Moreover, most of the electrons that leave will have energies close to the maximum range of 700–1000 eV.

Equation (3) was used to calculate the electron current I reaching the substrate during the deposition of CaF_2 films. This equation is derived based on the experimental conditions and the geometry of the CaF_2 deposition setup on the Si/SiO_2 substrate:

$$I = I_{cathode} \cdot k \cdot \beta, \quad (3)$$

where $I_{cathode}$ is the experimentally measured electron current of 0.023 A, and $k = 4{\cdot}10^{-3}$ is a coefficient that accounts for electron losses depending on the solid angle at which the substrate is viewed from the center of the pellet. As mentioned above, when the primary electron energy is 1000 eV, the sample is exposed to secondary electrons with energies close to 1000 eV. At this energy, the elastic and inelastic reflection coefficients for metals are typically less than or equal to 0.1. For molybdenum (atomic number 42), the reflection coefficient of these electrons $\beta = 0.06$ can be used [37]. By substituting the above coefficients into Equation (3), the current value I was estimated to be $5{\cdot}10^{-6}$ A.

Based on the above, it is possible to fill the traps of the SiO_2 layer with electrons during CaF_2 deposition on the Si/SiO_2 substrate. This results in the peaks in the PE spectra of the $Si/SiO_2/CaF_2$ structures due to the photoelectron emission from the traps present in the SiO_2 layer, according to the mechanism described in Ref. [35].

As demonstrated by Ref. [35], the integrated intensity of the photoelectron emission from the Si/SiO_2 substrate is directly proportional to the dose of electron irradiation. A similar correlation was observed for CaF_2 films with thicknesses ranging from 50 to 125 nm (Fig. 7). In this figure, the normalized integrated intensity is plotted, and calculated using the reference value corresponding to the CaF_2 thickness (125 nm) that exhibited the maximum integrated intensity observed in the measurements. At a thickness of 277 nm, the normalized integrated intensity decreased sharply (Fig. 7). The PE spectrum of the 277 nm thick film changed and became similar in shape and intensity to the bare Si/SiO_2 substrate (Fig. 5). The range of electron exposure doses shown in Fig. 7 was determined by the deposition time required to achieve the desired thicknesses of the CaF_2 films.

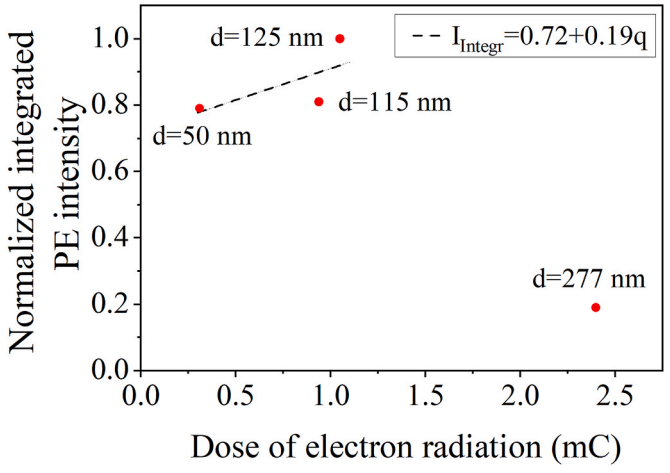

Fig. 7. Normalized integrated PE intensity ($I_{integr.}$) for CaF_2 films of different thicknesses (d) as a function of electron irradiation dose (q). The electron irradiation dose was determined by the deposition time of each CaF_2 film.

Previous studies [38,39] investigated the effect of medium energy electron irradiation (0.8–2.5 keV) on CaF_2 crystals. These studies have found that the formation of metallic calcium clusters in the crystals increased with the irradiation dose in the range of 0–1 mC until saturation occurred at around 2 mC. The metallic calcium clusters were not present in the crystal before irradiation. In addition, recent work [40] studied the influence of 1–8 eV electron bombardment on the CaF_2 surface and showed that the most intensive metallization occurs at electron energies of 2–3 eV. In our study (Fig. 7), a distinct change in the integrated intensity and shape of the PE spectrum is observed precisely at a dose of about 2.5 mC, which aligns with the saturation point reported in earlier studies.

The processes occurring in CaF_2 crystals under electron irradiation involve several steps. When fluorite-structured crystals are irradiated with fast electrons, an electron moves to the conduction band and forms an electron-hole (*e-h*) pair. The localization of the electron near the V_k center (a hole binding two neighboring anions into an F_2^- molecule) leads to the formation of an unrelaxed self-trapped exciton (STE) [41]. The relaxation of the STE results in the formation of an *F* center (an electron trapped by an anion vacancy) and an *H* center located in its proximity (an interstitial fluorine atom covalently bonded to a lattice anion) [42]. However, the probability of separation of such an *F–H* pair is very low. Optical excitation of the relaxed STE in the absorption region of the *H* center (4.5 eV for the CaF_2 crystal) results in the conversion of the STE into spatially separated *F–H* pairs [43]. Later, in Ref. [44], theoretical calculations confirmed the decomposition of the *F–H* pair into three defects: an *F* center, a V_k center, and an *I* center (an anion in an interstitial site).

According to Ref. [38], the mechanism described above can be achieved by exposing CaF_2 crystal to electrons with energies around 1 keV, which produces a spectrum of secondary electrons. This spectrum contains both fast electrons and slow true secondary electrons. When the fast part of the spectrum interacts with the crystal, relaxed STEs (*F–H* pairs) are formed. When the H center is excited by slow true secondary electrons with energies of 5 eV or greater, it separates into charged V_k and *I* centers. This process results in the formation of stable *F* centers and charged V_k and *I* centers. Stable *F* centers can combine to form metal clusters in CaF_2 crystals, but there must be a mechanism to prevent their recombination [38,45]. Moreover, the main factor influencing fluorine diffusion and leading to the formation of metal clusters in the volume and on the surface is the electric field generated in the crystal by electron irradiation.

The *I* and V_k centers have negative charges and are separated in the electric field. The V_k center has high mobility [46,47], resulting in a rapid spatial separation of V_k and *F* centers, effectively limiting their recombination. As mentioned, this leads to stable *F* and *I* centers forming, which is crucial to the metallization process.

The presence of an electric field in the CaF_2 layer facilitates the spatial separation of V_k and *F* centers. F centers can concentrate at the interface with SiO_2 and become ionized under the influence of electron irradiation.

As previously mentioned, there is a difference in the PE spectra between CaF_2 films with a thickness of 125 nm or less and 277 nm (Figs. 5 and 7), and the properties of films with different thicknesses are correlated to the dose of electron irradiation obtained during deposition. Accumulating a specific dose results in the appearance of calcium regions and changes in the distribution of defect centers in the CaF_2 layer.

To study the excitation and relaxation processes of PE spectra in the Si/SiO_2/CaF_2 structures, additional experiments were conducted. These structures were further irradiated with 1.5 keV electrons inside the vacuum chamber of the PE spectrometer, and the results demonstrated that the PE intensity changed insignificantly for the 50 nm and 125 nm thick films (Fig. 8(a) and (b)). However, the 277 nm thick film (Fig. 8(c)) exhibited PE peaks characteristic of samples with thicknesses equal to or less than 125 nm, and the intensity of these peaks increased with increasing irradiation dose.

After terminating the electron irradiation, the integrated PE intensity and the PE maxima remained stable for 24 h when the samples of all thicknesses were kept in a vacuum. However, when exposed to air, the integrated PE intensity decreased at different rates for samples of various thicknesses. The integrated PE intensity decreased 2.5 times in 24 h for the 50 nm and 125 nm thick samples, while all maxima were preserved in the spectrum. For the 277 nm thick samples, the integrated intensity of PE decreased 2.5 times in 2 h, and the maxima were not preserved.

Thus, the relaxation of PE intensity in CaF_2 films occurs only when the film's surface is exposed to the atmosphere. Reference [48] reported that chipping a CaF_2 crystal in air resulted in an increase of additional forbidden energy states compared to chipping it in a vacuum. When exposed to oxygen, an O^{2-} ion becomes embedded in the lattice of the CaF_2 crystal, causing the formation of (O^{2-}-V_A) defect center as an anion vacancy V_A appears nearby to restore neutrality [49]. This suggests that the absence of PE relaxation in a vacuum and the varying relaxation rates observed for CaF_2 films of different thicknesses in the air may be due to the formation of additional defects in the CaF_2 layer. As previously mentioned, the intensity of the PE maxima is related to the concentration of electrons in the electron traps of the SiO_2 layer. Therefore, the relaxation of the PE intensity depends on the transfer of electrons from the traps in SiO_2 to additional defects in the CaF_2 layer when exposed to the atmosphere. It was also demonstrated above that high doses of electron irradiation during the deposition of the 277 nm thick film may result in the region of increased concentration of ionized F centers, i.e., unfilled anion vacancies V_A, at the CaF_2–SiO_2 interface, which can form additional (O^{2-}-V_A) centers. The relaxation of the PE spectra intensity can be explained by the charge transfer transitions of electrons from SiO_2 traps to the CaF_2 layer by the mechanism described in Ref. [49]:

$$\left(O^{2-}\text{-}V_A\right) + e \rightarrow O^{2-}\text{-}F \rightarrow F_{2A}^{+}\left(O^{2-}\right), \tag{4}$$

where F_{2A}^{+} (O^{2-}) is the ionized pair of F centers distorted by the presence of O^{2-} ion.

As a result, due to the higher concentration of V_A vacancies, the PE relaxation rate for 277 nm thick samples is higher than for the 50 nm and 125 nm thick samples, where the separation of V_K and F centers does not occur, and the number of V_A vacancies is smaller.

It is essential to mention that the low PE intensity observed in the 277 nm thick film (Figs. 5 and 7) can also be theoretically explained by the large thickness of the film, which may prevent PE from the Si/SiO_2 substrate. However, this possibility is excluded by the appearance of PE peaks characteristic of the Si/SiO_2 substrate in the PE spectra of this film after additional electron irradiation (Fig. 8(c)). Furthermore, in Ref. [50], the passage of slow electrons through an epitaxial CaF_2 film grown on a Si substrate was investigated, and the PE from the substrate through an 800 nm thick CaF_2 film was recorded. The electron escape depth for CaF_2 was determined to be 260 nm, which is in agreement with our results.

Future research in this area could focus on experimental validation of the theoretical predictions by studying the optical properties of CaF_2 films deposited on SiO_2 substrates by electron beam evaporation, including luminescence, optical transmission, and defect-related

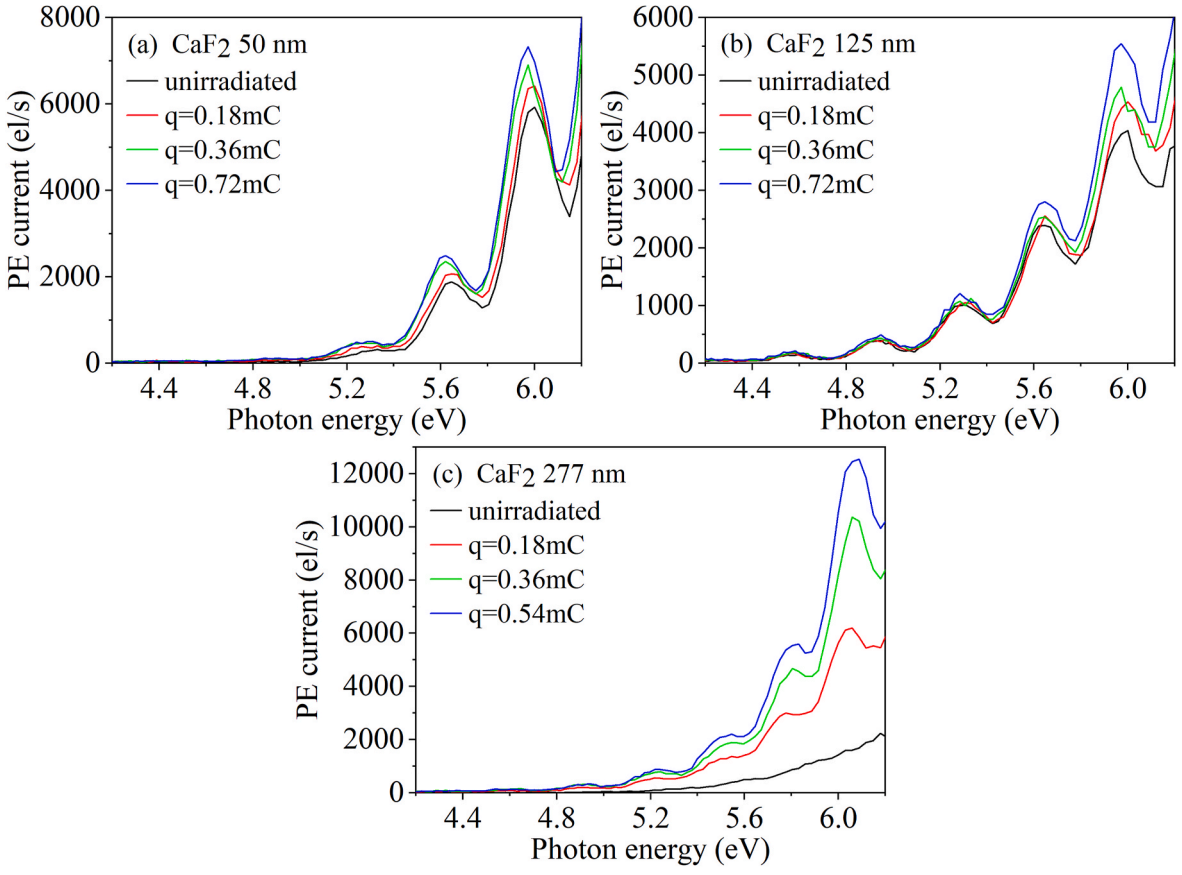

Fig. 8. PE spectra of (a) 50 nm, (b) 125 nm, and (c) 277 nm thick CaF_2 films on Si/SiO_2 substrate after additional electron irradiation with different doses (q).

absorption and emission due to metallic clusters, F centers, and other color centers.

4. Conclusions

Electron trapping in the SiO_2 layer during the electron beam deposition of CaF_2 thin films on the Si/SiO_2 substrate was studied using the PE technique. The deposition of the CaF_2 films was found to fill electron traps in the SiO_2 layer, resulting in characteristic maxima in the PE spectra. These maxima and the integrated PE intensity remained stable for at least 24 h when CaF_2 films of all thicknesses were kept in a vacuum. When exposed to air, the integrated PE intensity decreased by a factor of 2.5 over 24 h for films with a thickness of 125 nm or less, while all maxima remained in the spectra for several days. In contrast, for 277 nm thick films, the PE spectrum intensity relaxed to a low-intensity structureless curve within 2.5 h of air exposure.

These observations were explained by the proposed mechanism suggesting that the high irradiation dose obtained during the fabrication of the 277 nm thick film resulted in the formation of a region with an increased concentration of ionized F centers at the SiO_2–CaF_2 interface. Upon exposure to air, additional defects known as (O^{2-}-V_A) centers were formed. The intensity of the PE spectrum then underwent a relatively rapid relaxation due to electron transfer from SiO_2 traps to (O^{2-}-V_A) centers. In films with a thickness of 125 nm or less, the relaxation was much slower due to the lower concentration of ionized F centers. The study also confirmed the possibility of an electron escape depth of 260 nm [50] for CaF_2 material.

CRediT authorship contribution statement

Marina Romanova: Writing – original draft, Visualization, Methodology, Investigation, Funding acquisition, Formal analysis. **Sergii Chertopalov:** Writing – review & editing, Visualization, Investigation. **Yuri Dekhtyar:** Writing – review & editing, Resources, Formal analysis. **Ladislav Fekete:** Writing – review & editing, Visualization, Investigation. **Ján Lančok:** Writing – review & editing, Resources, Funding acquisition. **Michal Novotný:** Writing – review & editing, Funding acquisition. **Petr Pokorný:** Writing – review & editing, Investigation. **Anatoli I. Popov:** Writing – review & editing, Investigation. **Hermanis Sorokins:** Investigation, Writing – review & editing. **Aleksandr Vilken:** Writing – original draft, Methodology, Investigation, Formal analysis.

Declaration of competing interest

The authors declare that they have no known competing financial interests or personal relationships that could have appeared to influence the work reported in this paper.

Acknowledgement

This research was supported by the European Regional Development Fund under Project No. 1.1.1.2/VIAA/1/16/167, by Czech Science Foundation Project No. 20-21069S, and by Operational Programme Johannes Amos Comenius financed by European Structural and Investment Funds and the Czech Ministry of Education, Youth and Sports (Project No. CZ.02.01.01/00/22_008/0004596).

Data availability

I have shared the link to my data at the Attach File step.

Charge Trapping in SiO_2 Substrate during Electron Beam Deposition of CaF_2 Thin Films (Original data) (Mendeley Data)

References

[1] A.J. Stevenson, H. Serier-Brault, P. Gredin, M. Mortier, Fluoride materials for optical applications: single crystals, ceramics, glasses, and glass–ceramics, J. Fluor. Chem. 132 (2011) 1165–1173, https://doi.org/10.1016/j.jfluchem.2011.07.017.
[2] J. Chen, Z. Zhang, Y. Guo, J. Robertson, Electronic properties of CaF_2 bulk and interfaces, J. Appl. Phys. 131 (2022) 215302, https://doi.org/10.1063/5.0087914.
[3] C. Wen, M. Lanza, Calcium fluoride as high-k dielectric for 2D electronics, Appl. Phys. Rev. 8 (2021) 021307, https://doi.org/10.1063/5.0036987.
[4] L. Su, Y. Dong, W. Yang, T. Sun, Q. Wang, J. Xu, G. Zhao, Growth, characterization and optical quality of CaF_2 single crystals grown by the temperature gradient technique, Mater. Res. Bull. 40 (2005) 619–628, https://doi.org/10.1016/j.materresbull.2005.01.006.
[5] V. Pankratov, V. Pankratova, A.I. Popov, Luminescence and vacuum ultraviolet excitation spectroscopy of nanophosphors under synchrotron irradiation, Phys. Status Solidi B 259 (2022) 2100475, https://doi.org/10.1002/pssb.202100475.
[6] X. Li, X.A. Dou, H. Zhu, Y. Hu, X. Wang, Nanosecond laser-induced surface damage and its mechanism of CaF_2 optical window at 248 nm KrF excimer laser, Sci. Rep. 10 (2020) 5550, https://doi.org/10.1038/s41598-020-62469-y.
[7] J. Stäblein, K. Pöhl, A. Weisleder, G. vd Gönna, T. Töpfer, J. Hein, M. Siebold, Optical properties of CaF_2 and Yb^{3+}:CaF_2 for laser applications, Proc. SPIE-Int. Soc. Opt. Eng. 8080 (2011) 808002, https://doi.org/10.1117/12.886830.
[8] E.A. Kotomin, V.N. Kuzovkov, A.I. Popov, The kinetics of defect aggregation and metal colloid formation in ionic solids under irradiation, Radiat. Eff. Defect Solid 155 (2001) 113–125, https://doi.org/10.1080/10420150108214102.
[9] N.D. Quang, P.B.Q. Hieu, H. Kim, Pure CaF_2 crystal for fast neutron detection, Radiat. Phys. Chem. 221 (2024) 111756, https://doi.org/10.1016/j.radphyschem.2024.111756.
[10] F. Nakamura, T. Kato, G. Okada, N. Kawaguchi, K. Fukuda, T. Yanagida, Scintillation and dosimeter properties of CaF_2 transparent ceramic doped with Eu^{2+}, Ceram. Int. 43 (2017) 604–609, https://doi.org/10.1016/j.ceramint.2016.09.201.
[11] A.L. Pellegrino, E. Milan, A. Speghini, G. Malandrino, Fabrication of europium-doped CaF_2 films via sol-gel synthesis as down-shifting layers for solar cell applications, Materials 16 (2023) 6889, https://doi.org/10.3390/ma16216889.
[12] D. Hahn, Calcium fluoride and barium fluoride crystals in optics: multispectral optical materials for a wide spectrum of applications, Opt. Photonik 9 (2014) 45–48, https://doi.org/10.1002/opph.201400066.
[13] R. Assylbayev, A. Lushchik, C. Lushchik, I. Kudryavtseva, E. Shablonin, E. Vasil'chenko, M. Zdorovets, Structural defects caused by swift ions in fluorite single crystals, Opt. Mater. 75 (2018) 196–203, https://doi.org/10.1016/j.optmat.2017.10.026.
[14] R. Assylbayev, A. Akilbekov, A. Dauletbekova, A. Lushchik, E. Shablonin, E. Vasil'chenko, Radiation damage caused by swift heavy ions in CaF_2 single crystals, Radiat. Meas. 90 (2016) 18–22, https://doi.org/10.1016/j.radmeas.2015.12.034.
[15] A. Guille, A. Pereira, A. Bensalah-Ledoux, B. Moine, M. Novotný, J. Bulír J., P. Fitl, J. Lančok, Sensitization of Pr^{3+} ions by Eu^{2+} ions in CaF_2 thin films deposited by evaporation, J. Appl. Phys. 114 (2013) 203509, https://doi.org/10.1063/1.4836856.
[16] T. Zikmund, J. Bulír, M. Novotný, P. Jiříček, J. Houdková, J. Lančok, Electric and magnetic dipole emission of Eu^{3+}: effect of proximity to a thin aluminum film, J. Lumin. 246 (2022) 118778, https://doi.org/10.1016/j.jlumin.2022.118778.
[17] S. Stepanov, E. Chinkov, A. Shrayber, V. Shtan'ko, Transient optical absorption in calcium fluoride crystals, Radiat. Phys. Chem. 191 (2022) 109889, https://doi.org/10.1016/j.radphyschem.2021.109889.
[18] B.G. Ravi, S. Ramasamy, Status of study of colour centers in calcium fluoride, Int. J. Mod. Phys. B 6 (1982) 2809–2836, https://doi.org/10.1142/S0217979292002255.
[19] F. Gan, Y.N. Xu, M.Z. Huang, W.Y. Ching, J.G. Harrison, Optical properties of a CaF_2 crystal, Phys. Rev. B 45 (1992) 8248–8255, https://doi.org/10.1103/PhysRevB.45.8248.
[20] D. Ochs, M. Brause, S. Krischok, P. Stracke, W. Maus-Friedrichs, V. Puchin, A. Popov, V. Kempter, Characterization of LiF and CaF_2 surfaces using MIES and UPS (HeI), J. Electron. Spectrosc. Relat. Phenom. 88–91 (1998) 725–732, https://doi.org/10.1016/S0368-2048(97)00216-8.
[21] R.I. Eglitis, J. Purans, A.I. Popov, R. Jia, Tendencies in ABO_3 perovskite and SrF_2, BaF_2 and CaF_2 bulk and surface F-center ab initio computations at high symmetry cubic structure, Symmetry 13 (2021) 1920, https://doi.org/10.3390/sym13101920.
[22] J. Rivory, S. Fisson, V.N. Van, G. Vuye, Y. Wang, F. Abelés, K. Yu-Zhang, Study of CaF2 growth on Si, a-Si O_2 by in-situ spectroscopic ellipsometry, Thin Solid Films 233 (1993) 260–263, https://doi.org/10.1016/0040-6090(93)90103-V.
[23] N.E. Cetin, S. Korkmaz, S. Elmas, N. Ekem, S. Pat, M.Z. Balbağ, E. Tarhan, S. Temel, M. Özmumcu, The structural, optical and morphological properties of CaF_2 thin films by using Thermionic Vacuum Arc (TVA), Mater. Lett. 91 (2013) 175–178, https://doi.org/10.1016/j.matlet.2012.07.086.
[24] A.A. Velichko, V.A. Ilyushin, A.Y. Krupin, N.I. Filimonova, I.E. Rudenko, Effect of substrate on the photoluminescence spectra of CaF_2/Si multilayer structures, J. Surf. Invest.: X-ray, Synchrotron Neutron Tech. 17 (2023) 921–925, https://doi.org/10.1134/S1027451023040328.
[25] J.P. Ganachaud, C. Attard, R. Renoud, Study of the space charge induced by an electron beam in an insulating target, Phys. Status Solidi B 199 (1997) 175–184, https://doi.org/10.1002/1521-3951(199701)199:1%3C175::AID-PSSB175%3E3.0.CO;2-%23.

[26] E.I. Rau, A.A. Tatarintsev, E.Y. Zykova, Influence of ion implantation and electron pre-irradiation on charging of dielectrics under electron beam irradiation: application to SiO_2, Nucl. Instrum. Methods Phys. Res., Sect. B 460 (2019) 141–146, https://doi.org/10.1016/j.nimb.2018.12.030.
[27] W.Q. Li, C.Y. Mu, Charging effects of SiO_2 thin film on Si substrate irradiated by penetrating electron beam, Micron 140 (2021) 102961, https://doi.org/10.1016/j.micron.2020.102961.
[28] M.A. Stevens-Kalceff, K.J. Levick, The assessment of microscopic charging effects induced by focused electron and ion beam irradiation of dielectrics, Microsc. Res. Tech. 70 (2007) 195–204, https://doi.org/10.1002/jemt.20399.
[29] M.A. Knyazev, D.M. Sedlovets, O.V. Trofimov, A.N. Redkin, The influence of the electron-beam exposure of SiO_2/Si and quartz substrates on the selective growth of graphene-like films, Mater. Res. Bull. 86 (2017) 322–326, https://doi.org/10.1016/j.materresbull.2016.11.007.
[30] T.H. Ning, Electron trapping in SiO_2 due to electron-beam deposition of aluminum, J. Appl. Phys. 49 (1978) 4077–4082, https://doi.org/10.1063/1.325368.
[31] P.S. Vergeles, YuO. Kulanchikov, E.B. Yakimov, Charging effects in Al-SiO_2-p-Si structures after low-energy electron beam irradiation, J. Electron. Mater. 49 (2020) 5178–5183, https://doi.org/10.1007/s11664-020-08080-3.
[32] W. Primak, H. Kaufman, R. Ward, X-Ray diffraction studies of systems involved in the preparation of alkaline earth sulfide and selenide phosphors, J. Am. Chem. Soc. 70 (1948) 2043–2046, https://doi.org/10.1021/ja01186a018.
[33] Standard X-Ray Diffraction Powder Patterns, National Bureau of Standards, U.S., 1985. Monograph 25 Section 21 — Data for 92 Substances.
[34] The International XPS Database of Monochromatic XPS Reference Spectra, Calcium (Ca) & calcium compounds. https://xpsdatabase.net/calcium-ca-z20-chemicals/, 2024. (Accessed 23 December 2024).
[35] Y. Dekhtyar, G. Enichek, M. Romanova, B. Schmidt, A. Vilken, T. Yager, A. Zaslavski, Charge trap analysis of nanolayer Si_3N_4 and SiO_2 by electron irradiation assisted photoelectron emission, Phys. B 586 (2020) 412123, https://doi.org/10.1016/j.physb.2020.412123.
[36] E.M. Purcell, D.J. Morin, Electricity Ang Magnetism, third ed., Cambridge University Press, 2013.
[37] G. Gergely, Elastic peak electron spectroscopy, Scanning 8 (1986) 203–214, https://doi.org/10.1002/sca.4950080503.
[38] R. Bennewitz, D. Smith, M. Reichling, Bulk and surface processes in low-energy-electron-induced decomposition of CaF_2, Phys. Rev. B 59 (1999) 8237–8256, https://doi.org/10.1103/PhysRevB.59.8237.
[39] M. Reichling, The role of defect diffusion and metallization for electron-stimulated desorption from CaF_2, Nucl. Instrum. Methods Phys. Res., Sect. B 101 (1995) 108–114, https://doi.org/10.1016/0168-583X(95)00297-9.
[40] A.A. Abduvayitov, D.A. Tashmukhamedova, B.E. Umirzakov, A.T. Mamamdalimov, Effect of electron bombardment on the composition and structure of CaF_2/Si(111) films, J. Surf. Invest. 18 (2024) 491–494, https://doi.org/10.1134/S1027451024020228.
[41] R. Lindner, M. Reichling, R.T. Williams, E. Matthias, Femtosecond laser pulse excitation of electrons and excitons in CaF_2 and SrF_2, J. Phys. Condens. Matter 13 (2001) 2339–2346, https://doi.org/10.1088/0953-8984/13/10/324.
[42] K. Tanimura, Femtosecond time-resolved spectroscopy of the formation of self-trapped excitons in CaF_2, Phys. Rev. B 63 (2001) 184303, https://doi.org/10.1103/PhysRevB.63.184303.
[43] T. Eshita, K. Tanimura, N. Itoh, Photo-induced transformation of close Frenkel pairs in strontium fluorite, Phys. Status Solidi B 122 (1984) 489–500, https://doi.org/10.1002/pssb.2221220213.
[44] K.S. Song, Exciton relaxation in KBr and CaF_2 at low temperature: molecular dynamics study, Low Temp. Phys. 29 (2003) 754–758, https://doi.org/10.1063/1.1614185.
[45] M. Huisinga, N. Bouchaala, R. Bennewitz, E.A. Kotomin, M. Reichling, V. N. Kuzovkov, W. Von Niessen, The kinetics of CaF_2 metallization induced by low-energy electron irradiation, Nucl. Instrum. Methods Phys. Res., Sect. B 141 (1998) 79–84, https://doi.org/10.1016/S0168-583X(98)00065-2.
[46] W. Hayes, Crystals with the Fluorite Structure: Electronic, Vibrational and Defect Properties, Clarendon Press, Oxford, 1974.
[47] N. Chuklina, A. Mysovsky, Theoretical study of self-trapped hole diffusion in CaF_2, SrF_2, BaF_2 crystals, Radiat. Meas. 128 (2019) 106135, https://doi.org/10.1016/j.radmeas.2019.106135.
[48] M. Reichling, M. Huisinga, S. Gogoll, C. Barth, Degradation of the CaF_2 (111) surface by air exposure, Surf. Sci. 439 (1999) 181–190, https://doi.org/10.1016/S0039-6028(99)00760-8.
[49] A.S. Mysovsky, E.A. Radzhabov, M. Reichling, A.L. Shluger, P.V. Sushko, Optical properties and transformation mechanism of oxygen centres and their aggregates in CaF_2 crystals, Phys. Status Solidi C 2 (2005) 392–396, https://doi.org/10.1002/pssc.200460191.
[50] B. Quiniou, W. Schwarz, Z. Wu, R.M. Osgood, Q. Yang, J.M. Phillips, Photoemission from thick overlying epitaxial layers of CaF_2 on Si (111), Appl. Phys. Lett. 60 (1992) 183–185, https://doi.org/10.1063/1.106957.